VOL. 2, NO. 3, MAY-JUNE 1979 J. GUIDANCE AND CONTROL 221
ARTICLE NO. 79-4066

A Rationale for Human Operator Pulsive Control Behavior

Ronald A. Hess*
NASA Ames Research Center, Moffett Field, Calif.

When performing tracking tasks which involve demanding controlled elements such as those with K/s^2 dynamics, the human operator often develops discrete or pulsvie control outputs. Although such pulsive control behavior has been linked to the necessity for low-frequency lead equalization on the part of the human operator, no satisfactory model-based explanation of pulsive behavior has been offered to date. A dual-loop model of the human operator is discussed, the dominant adaptive feature of which is the explicit appearance of an internal model of the manipulator-controlled element dynamics in an inner feedback loop. Using this model, a rationale for pulsive control behavior is offered which is based upon the assumption that the human attempts to reduce the computational burden associated with time integration of sensory inputs. It is shown that such time integration is a natural consequence of having an internal representation of the K/s^2-controlled element dynamics in the dual-loop model. A digital simulation is discussed in which a modified form of the dual-loop model is shown to be capable of producing pulsive control behavior qualitively comparable to that obtained in experiment.

Nomenclature

d = disturbance
e = $-(m+d)$, error
e_d = $Y_d e$, displayed error
j = imaginary unit
k = integer exponent appearing in $Y_{p_{\dot{m}}}$
K = controlled element gain
K_e = gain appearing in Y_{p_e}
$K_{\dot{m}}$ = gain appearing in $Y_{p_{\dot{m}}}$, s
K_s = gain appearing in crossover approximation to $Y_\delta Y_c$
m = controlled element output due to control activity
$\hat{m}$ = human operator's estimate of $\dot{m}$, s^{-1}
n_e = injected error remnant
s = Laplace variable
T_L = lead time constant appearing in Y_{p_e}, s
$T_{\dot{m}}$ = washout time constant appearing in $Y_{p_{\dot{m}}}$, s
u_c = $u_e - u_{\dot{m}}$
u_c' = output of Y_{p_u}
u_e = output of Y_{p_e}
$u_{\dot{m}}$ = output of $Y_{p_{\dot{m}}}$
u_δ = force output of neuromuscular system
Y_δ = manipulator dynamics
$\hat{Y_\delta Y_c}$ = human operator's model of manipulator-controlled element dynamics
Y_c = controlled element dynamics
Y_d = display dynamics
Y_p = human operator single-loop describing function
Y_{p_e} = outer-loop equalization dynamics in dual-loop human operator model
$Y_{p_{\dot{m}}}$ = inner-loop equalization dynamics in dual-loop human operator model
Y_{p_n} = human operator neuromuscular dynamics
Y_{p_u} = nonlinear element in dual-loop human operator model
δ = manipulator output
ζ_n = neuromuscular system damping ratio
α, β = parameters which determine characteristics of Y_{p_u}
ρ_a^2 = relative correlated output
σ_x = root-mean-square value of variable x
τ = time delay, s
Φ_{xx} = power spectral density of variable x
ω = frequency, rad/s
ω_n = neuromuscular system undamped natural frequency, rad/s

Received March 27, 1978; revision received July 19, 1978. This paper is declared a work of the U.S. Government and therefore is in the public domain.
Index category: Handling Qualities, Stability and Control.
*Research Scientist. Member AIAA.

Introduction

WHEN performing a single-axis compensatory tracking task such as that represented in Fig. 1, human operator manipulator output characteristics are a strong function of the form of the controlled element. When relatively non-demanding controlled elements are involved, such as those with K or K/s dynamics, manipulator output is essentially smooth and uniform. Disturbances with Gaussian amplitude distributions give rise to manipulator outputs which are also Gaussian. However, when demanding controlled elements such as those with K/s^2 dynamics are involved, the human operator often develops a more discrete or pulsive manipulator output. Gaussian disturbances often yield manipulator outputs which exhibit bimodal amplitude distributions such as shown in Fig. 2.

In terms of single-loop, linear, frequency domain models of the human operator, pulsive control behavior has been associated with the need for low-frequency lead equalization on the part of the human.[1] Beyond this, however, the linear single-loop models now in common use cannot, of themselves, produce pulsive manipulator outputs. Although nonlinear models have been developed which exhibit pulsive behavior,[1-4] all the models share the common problem of being somewhat disjoint from the quasilinear representations of the human operator which satisfactorily explain human control activity with less demanding controlled elements. The nonlinearities in these models possess somewhat tenuous *raisons d'etre,* and as such, do not lead to satisfactory model-based rationales for pulsive control behavior.

Using a model structure introduced by Smith,[5,6] Hess has recently developed a "dual-loop" model of the human controller.[7] In the research to be described, it will be shown that this model can offer a rationale for pulsive control behavior which has its basis in the structure of the model itself and in the assumption that the human attempts to reduce the computational burden associated with time integration of sensory inputs.

Dual-Loop Model

A block diagram of the dual-loop model, whose name derives from the existence of an inner feedback loop, is shown in Fig. 3. In Ref. 7 this model was shown capable of producing human operator describing functions closely

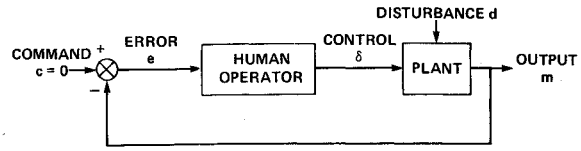

Fig. 1 Single-axis compensatory tracking task.

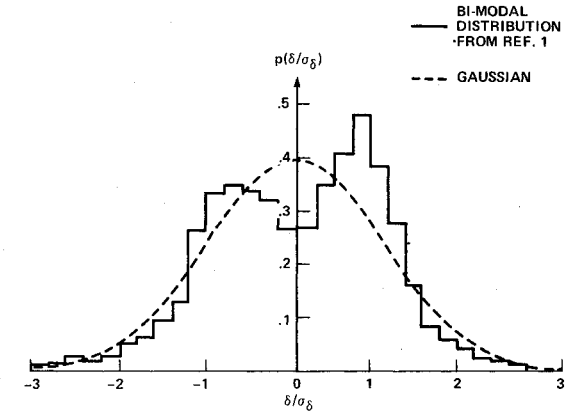

Fig. 2 Human operator bimodal manipulator output amplitude distribution.

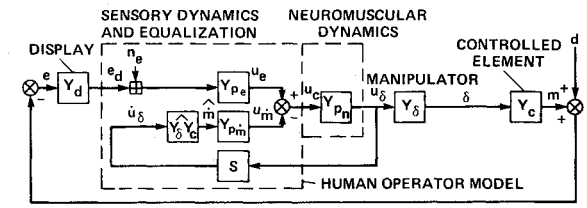

Fig. 3 Quasilinear dual-loop model of the human operator.

approximating those measured in a series of compensatory tracking tasks which varied considerably in terms of ease of control. The sensory inputs to the human in the model of Fig. 3 are displayed error e_d and control force u_δ. The sensory modality for displayed error can be visual, aural, or tactile. The control force is assumed to be sensed kinesthetically.

The function of the inner loop in the model of Fig. 3 is to feed back equalized output rate $u_{\dot m}$ to the neuromuscular system Y_{p_n}. The remaining portion of the neuromuscular command signal is equalized error, u_e. Table 1 shows the form of each of the elements of the model. Details can be found in Ref. 7.

Implicit in the dual-loop formulation is the assumption that the structure as outlined in Table 1 is complete; i.e., no additions must be made or restructuring undertaken to account for the effects of various controlled elements, displays, manipulators, and so on. The adaptive potential of the model is contained in the parameters of the inner- and outer-loop equalization and in the internal manipulator-controlled element model $Y_\delta \hat{Y}_c$. Indeed, the dominant adaptive feature of the model is the explicit appearance of $Y_\delta \hat{Y}_c$ in the equivalent single-loop form of the model (Y_p) in Table 1.

In Ref. 7, five hypotheses regarding the general adaptive characteristics of the parameterized dual-loop model were offered. The last of these hypotheses is pertinent to this discussion and is repeated here for convenience.

Hypothesis 5. The transfer function $\hat{m}/u_\delta$ which describes part of the equalization activity in the inner loop of the dual-loop model is of the form: $\hat{m}/u_\delta = sY_\delta \hat{Y}_c = sK_s s^n$ ($n=0, \pm 1, \pm 2, \ldots$, etc). The frequency characteristics of $Y_\delta Y_c$ in the region beyond the open-loop crossover frequency can be used to determine K_s and n.

Table 2 shows the model parameters selected in Ref. 7 to give acceptable comparisons between the experimental and

Table 1 Dual-loop model parameters

Expression	Description
$Y_{p_e} = K_e (T_L s+1) e^{-\tau s}$	Displayed error equalization
$Y_{p_{\dot m}} = \dfrac{K_{\dot m} [(T_{\dot m}/\lvert T_{\dot m}\rvert s]^k}{(T_{\dot m} s+1)^k}$	Control rate equalization, $k=1,2,\ldots$
$Y_\delta \hat{Y}_c$	Human controller's internal model of manipulator-controlled element dynamics
$Y_{p_n} = \dfrac{1}{(s/\omega_n)^2 + (2\zeta_n/\omega_n)s+1}$	Neuromuscular dynamics
n_e	Remnant injected into displayed error
$Y_p = \dfrac{u_\delta}{e_d} = \dfrac{Y_{p_e} Y_{p_n}}{1 + Y_{p_n} Y_\delta \hat{Y}_c Y_{p_{\dot m}} s}$	Equivalent single-loop human controller describing function

model-generated describing functions for the controlled elements indicated. The reader is referred to Ref. 7 for the sources of the experimental data. Note that the last two rows of the table indicate that simplified internal models for the manipulator-controlled element dynamics have been used in matching the experimental data, as per Hypothesis 5.

The fifth hypothesis is central to the discussion of pulsive control behavior which is to follow. In terms of the dual-loop model, the hypothesis implies that the human operator can generate the inner-loop feedback signal $\hat{m}(t)$ by differentiating, multiplying by a constant, or integrating the force applied to the manipulator, $u_\delta(t)$. In this light, the internal model of the manipulator-controlled element dynamics $Y_\delta \hat{Y}_c$ merely determines which of these time domain operations is appropriate for the task at hand.

As a concrete example, consider internal models of the form, $Y_\delta \hat{Y}_c = K$, K/s and K/s^2, which encompass *all* of the controlled element dynamics in Table 2. With $Y_\delta \hat{Y}_c = K$ (row 1, Table 2)

$$\hat{m} = sY_\delta \hat{Y}_c u_\delta = Ksu_\delta$$

or, in the time domain,

$$\hat{m}(t) = K\mathrm{d}u_\delta(t)/\mathrm{d}t \tag{1}$$

With $Y_\delta \hat{Y}_c = K/s$ (row 2, Table 2)

$$\hat{m} = sY_\delta \hat{Y}_c u_\delta = Ku_\delta$$

or

$$\hat{m}(t) = Ku_\delta(t) \tag{2}$$

With $Y_\delta \hat{Y}_c = K/s^2$ (rows 3-5, Table 2)

$$\hat{m} = sY_\delta \hat{Y}_c u_\delta$$

or

$$\hat{m}(t) = K\int_0^t u_\delta(t)\,\mathrm{d}t \tag{3}$$

From what is known about the general structure of the human neuromuscular system, it is quite probable that only the last of the time domain operations of Eqs. (1-3) need involve actual "computational activity" in the higher levels of

Table 2 Summary of dual-loop modeling results from Ref. 7

$Y_\delta Y_c$	$\hat{Y}_\delta \hat{Y}_c$	K_e	T_L, s	$K_{\dot{m}}$, s	$T_{\dot{m}}$, s	τ, s	ζ_n	ω_n, rad/s	k
1.0	1.0	2.5	0	0.5	1.0	0.1	0.1	20	1
$1/s$	$1/s$	18.0	0	6.0	2.0	0.13	0.3	15	1
$1/s^2$	$1/s^2$	26.5	0	32.3	3.33	0.16	0.7	15	1
$2.82/s(s-1)$	$2.82/s^2$	5.5	0.33	10.0	5.0	0.15	0.1	15	3
$145/\Delta$[a]	$10/s^2$	1.4	0	1.0	1.25	0.19	0.7	15	1

[a] $\Delta = s^3 + 12.3s^2 + 11.6s$.

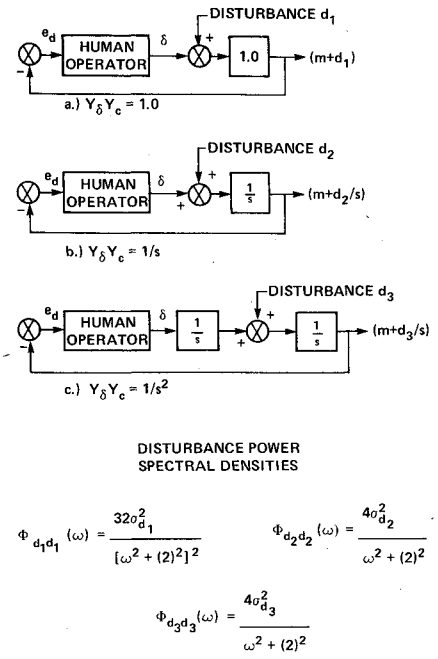

Fig. 4 Block diagrams of three experimental tracking tasks.

the nervous system. The muscular activity associated with tracking tasks such as those to be discussed here can be characterized by changes in the length and tension of the agonist/antogonist muscle pairs which drive the manipulator. These changes occur about some average operating point. Changes in length arise from manipulator movement and tendon/interface compliance, both of which are a consequence of the generation of tension (control force). Changes in tension and *rates* of change in tension can be sensed by the Golgi tendon organs, while changes in length and *rates* of change in length can be sensed by the muscle spindles.[8,9] Furthermore, the results of this sensory activity can be transmitted to higher levels of the nervous system where other sensory inputs converge (e.g., a visual input providing $e_d(t)$). This means, for example, that the *operation* of differentiation implied by Eq. (1) may well be obviated. The same cannot be said for the integration operation, however. Since there exist no proprioceptors in the human neuromuscular system whose output is proportional to the integral of muscle tension, the integration in Eq. (3) must be accomplished in higher levels of the nervous system; i.e., in terms of a dual-loop model, the operation of Eq. (3) must be taken in a literal sense, constituting a considerable computational burden.

The requirement for precise integration of $u_\delta(t)$ is eased somewhat by the fact that integration errors of relatively low frequency (i.e., "drift") are not of great significance in the dual-loop model. This is attributable to the low-frequency washout characteristics of $Y_{p_{\dot{m}}}$ (see Table 1) and to the presence of the outer error-feedback loop in the model, both of which mitigate the effect of low-frequency integration errors on tracking performance. However, the matter is complicated by the fact that the controlled element dynamics

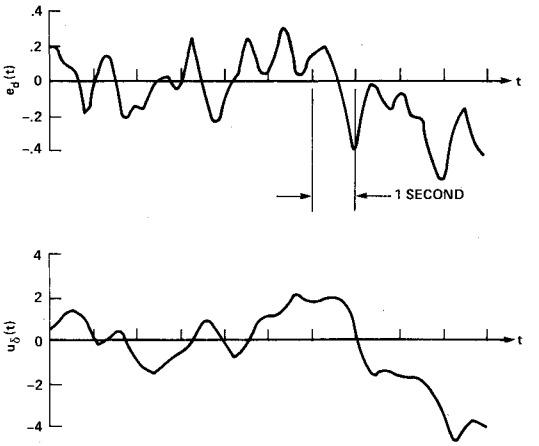

Fig. 5 Error and control force from dual-loop model, $Y_\delta Y_c = K$.

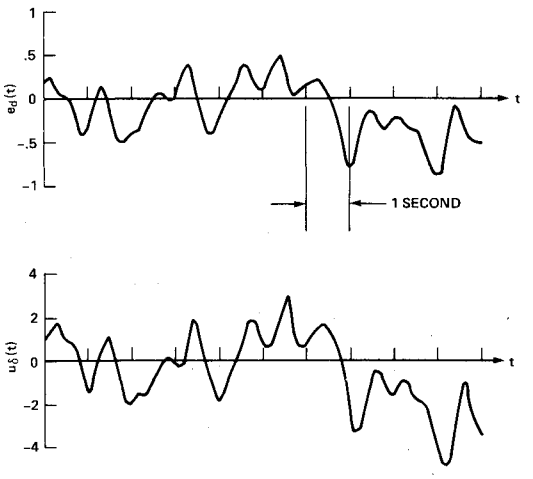

Fig. 6 Error and control force from dual-loop model, $Y_\delta Y_c = K/s$.

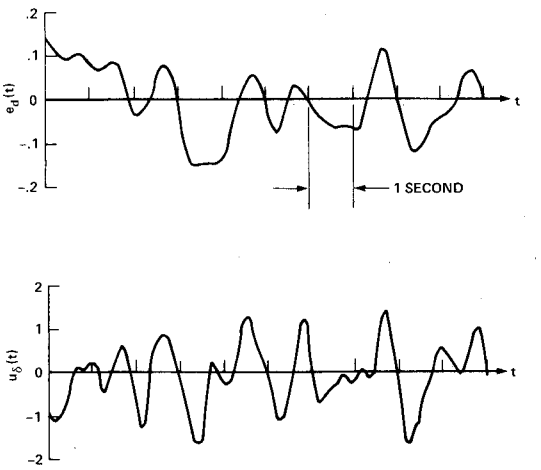

Fig. 7 Error and control force from dual-loop model, $Y_\delta Y_c = K/s^2$.

which (according to the dual-loop model) require integration of the control force are also those which demand the largest inner-loop activity, as quantified by $K_{\dot{m}}/K_e$ (see Table 2). Thus, on the one hand, considerable inner-loop activity in the form of time integration is necessary to maintain acceptable performance or even stability with controlled elements such as those shown in the last three rows of Table 2, while on the other hand, such time integration can be a considerable computational burden to the human. It is the thesis of this research that pulsive control behavior represents an attempt by the human operator to generate control forces which are *more easily time integrable* than those which would exist in the absence of pulsing. "Ease of integrability" can be generally interpreted in a physiological sense as applying to those waveforms whose integration requires a minimum of higher-level activity in the central nervous system. It should be pointed out that the concept of explaining pulsive control behavior as a means of easing the computational burden of control force integration was first suggested by Young and Meiry over a decade ago.[3] Their explanation, however, did not include a human operator model whose structure explicitly cited the need for control force integration.

Digital Simulation

To aid in the discussion of pulsive control behavior, a digital simulation of the three compensatory tracking tasks shown in Fig. 4 was implemented. These tasks, taken from Ref. 10, employ controlled element dynamics of K, K/s, and K/s^2, and are identical to those used to obtain the dual-loop model parameters in the first three rows of Table 2. In the simulation, the human operator was represented by the dual-loop model with the appropriate parameter values of Table 2. The random disturbances, $d_i(t)$ $(i=1,2,3)$, were represented by sums of ten sinusoids whose amplitudes and frequencies were chosen to match the frequency distribution of power in the appropriate power spectral densities shown in Fig. 4 and used in Ref. 10. Although an empirical model for injected error remnant was developed in Ref. 7, no remnant injection was included in the simulation for the sake of simplicity. Figures 5-7 show approximately 10 s of simulation time histories for displayed error $e_d(t)$ and applied manipulator force (or more simply, control force) $u_\delta(t)$ for the three controlled element dynamics shown in Fig. 4.

For the pure gain controlled element, the control force time history of Fig. 5 is relatively smooth, with little high-frequency content. Sensing and utilizing control rate should not be too demanding on the human operator, especially since little inner-loop activity is required for the pure gain dynamics as quantified by $K_{\dot{m}}/K_e = 0.2$.

For the K/s controlled element dynamics, the control force time history of Fig. 6 has virtually the same frequency content as the error signal. This is not surprising since the equivalent single-loop form of the dual-loop model resembles a pure gain with time delay in the region of open-loop crossover. The required operation is simply multiplication by a constant which should pose no difficulty for the human operator.

For the K/s^2 controlled element dynamics, the control force time history of Fig. 7 is quite oscillatory in nature. The required operation of integrating $u_\delta(t)$ in Fig. 7 is accompanied by a relatively large amount of inner-loop activity as quantified by $K_{\dot{m}}/K_e = 1.22$. It has been suggested that these requirements pose difficulties for the human operator and lead to pulsive control behavior.

Human Operator Pulsive Behavior

No time histories of human operator control activity were reported in Ref. 10. However, Fig. 8 shows a pair of manipulator force time histories taken from Refs. 1 and 4 where K/s^2 controlled element dynamics were utilized.

An examination of Figs. 7 and 8 reveals two important facts. First, as defined by the existence of discrete control movements and obviously bimodal amplitude distributions,

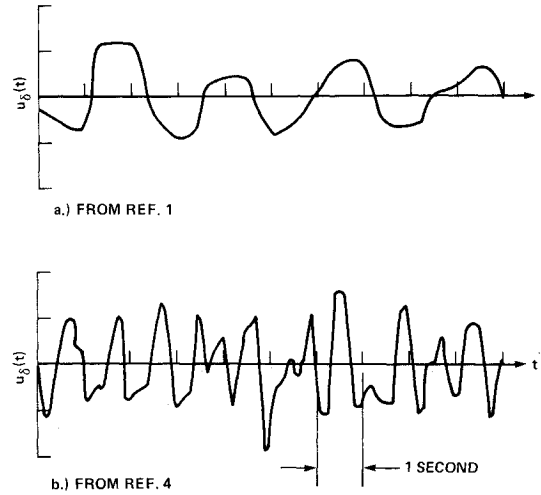

Fig. 8 Pulsive control behavior from experiments of Refs. 1 and 4.

the time histories of Fig. 8 are pulsive in nature while that of Fig. 7 is not. Second, the two pulsive time histories of Fig. 8 differ considerably in waveform and frequency. Fig. 8a shows somewhat periodic control pulses, each of approximately 1.25 s average duration. Figure 8b consists of a train of impulsive-type control forces, each with an average duration of approximately 0.45 s.

As pointed out in Ref. 3, the manner in which pulsive time histories such as those in Fig. 8 can ease the computational burden of integration is inherent in the discrete nature of the pulses themselves. For example, with pulsive control, Eq. (3) can be written

$$\hat{m}(t) = K\int_{t-\Delta T_{n-1}}^{t} u_\delta(t)\,dt + K\int_{t-\Delta T_{n-1}-\Delta T_{n-2}}^{t-\Delta T_{n-1}} u_\delta(t)\,dt + \ldots \tag{4}$$

where ΔT_i is the duration of the ith pulse of $u_\delta(t)$. With A_i representing the average amplitude (with sign) of the ith pulse of $u_\delta(t)$, Eq. (4) can be rewritten as

$$\hat{m}(t) \doteq \sum_{i=1}^{n} A_i \Delta T_i \tag{5}$$

The computational aspects of Eq. (5) are considerably simpler than those implied by Eq. (3), especially as applied to the nonpulsive control activity of Fig. 7.

Dual-Loop Model Pulsive Behavior

It is pertinent to determine whether a modification of the dual-loop model will allow pulsive control force time histories to be generated in a digital simulation similar to that just discussed. As Fig. 7 indicates, pulsive behavior does not occur naturally with the structure of Fig. 3 and the parameter values of Table 2. This is because the inclusion of $Y_\delta \hat{Y}_c = K/s^2$ in the frequency domain form of the model is equivalent to an assumption of perfect integration capability in the time domain. The computational burden associated with such a capability has just been postulated as the underlying cause of pulsive control behavior in the human operator.

The rationale for pulsive behavior which has been offered here would be seriously weakened if it were found that the only way to produce more easily integrable control forces in the model was to include model elements which implied complex or unrealistic signal processing and control activity on the part of the human. Consequently, in attempting to induce pulsive control behavior in the dual-loop model, the following criteria were borne in mind: first, the pulsive control behavior should be qualitatively similar to that of Fig. 8 (i.e., it should match the available data); and second, there should be as few new parameters as possible introduced into

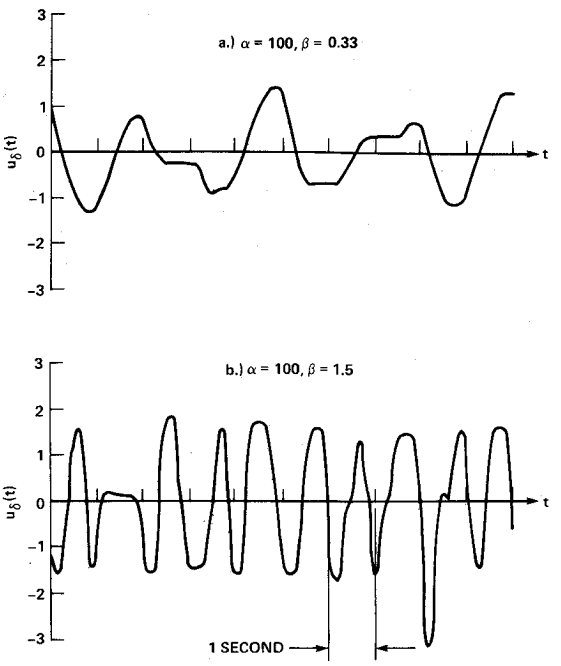

Fig. 9 Pulsive control behavior from dual-loop model, $Y_\delta Y_c = K/s^2$.

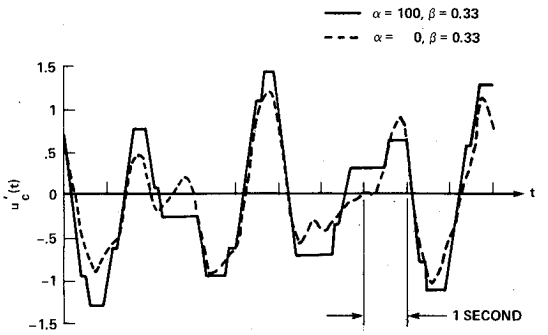

Fig. 10 Neuromuscular command for modified dual-loop model, $Y_\delta Y_c = K/s^2$.

Table 3 Relative correlated output for modified dual-loop model $Y_\delta Y_c = K/s^2$

α	β	ρ_a^2
0	1.0	1.0
100	0.33	0.95
100	1.5	0.77

the existing model structure. Also, the model modifications should not imply unrealistic information processing and control activity. Finally, the closed-loop model performance should be relatively insensitive to variations in the parameters of the new element or elements which are used to produce pulsive behavior.

Fortunately, the addition of a single nonlinear element Y_{p_u} immediately before the neuromuscular dynamics of the dual-loop model of Fig. 3 allows the preceding criteria to be met, albeit probably not uniquely. The characteristics of Y_{p_u} are given by

$$\begin{aligned} \dot{u}_c' &= 0 \quad \text{for} \quad |\dot{u}_c| < \alpha \\ u_c' &= \beta u_c \quad \text{for} \quad |\dot{u}_c| \geq \alpha \end{aligned} \tag{6}$$

where u_c and u_c' are respectively the input and output of the nonlinear element Y_{p_u}. The three criteria were met as follows. First, as will be seen, by varying *only* the values of the parameters α and β and by utilizing the remaining model parameter values in the third row of Table 2, pulsive control time histories which approximate those of Fig. 8 can be obtained from the digital simulation of the dual-loop model. Other nonlinear characteristics such as relay or toggle nonlinearities[11] were found to produce unrealistic control amplitude distributions with nearly all control activity occurring at the relay limits. Second, as Eqs. (6) indicate, the nonlinearity Y_{p_u} is parameterized by only two quantities, α and β, and does not imply unrealistic human information processing and control activity. The action of Y_{p_u} merely causes $u_c'(t)$ to remain constant until a sufficiently rapid change in $u_c(t)$ occurs. The magnitude of α will be such that the implied necessity of discriminating the criterion value of $\dot{u}_c(t)$ would pose no difficulty for the human. Finally, the position of Y_{p_u} in the forward part of an inner feedback loop possessing a relatively large feedback gain ($K_{\dot{m}}$) tends to minimize the effect of variations in α and β about their nominal values.

Figure 9 shows the control force time histories from the dual-loop model simulation using the indicated values of α and β. The rest of the dual-loop model parameters are identical to those used in obtaining the time histories of Fig. 7. As in the case of the linear model, no remnant injection was included in the simulation. The particular α and β values of Fig. 9 are the result of an informal iterative procedure in which the waveform of Fig. 7 was transformed into two waveforms each of which approximated one of the pulsive control time histories shown in Fig. 8. The average pulse duration of Fig. 9a is approximately 1.25 s, while that of Fig. 9b is approximately 0.5 s. No attempt was made at more exact reproduction of the experimental waveforms of Fig. 8 since the pertinent nominal dual-loop model parameters of Table 2 were selected on the basis of describing function measurements from an experiment in Ref. 10 with similar controlled element dynamics but with manipulator and disturbance characteristics which differed from those used in the experiments of Refs. 1 and 4.

The magnitude of the α parameter ($\alpha = 100$) belies its rather subtle effect on the waveform of $u_c'(t)$ as indicated in Fig. 10. Here, simulation time histories of $u_c'(t)$ are shown for $\alpha = 0$, $\beta = 0.33$ (effectively *no* nonlinearity) and for $\alpha = 100$, $\beta = 0.33$. The large α value produces a discrete neuromuscular command time history with an overall waveform which is slightly more oscillatory than that with $\alpha = 0$, but which still exhibits a strong lineage with the linear system. A quantitive measure of the closed-loop effect of the nonlinearity can be found in a quantity called the "relative correlated output" (referred to as ρ_a^2), defined as that portion of the power in the model output $u_\delta(t)$ which exists at the disturbance frequencies, divided by the total power in $u_\delta(t)$.[1] Table 3 shows the ρ_a^2 values resulting from the digital simulation of the linear and nonlinear forms of the dual-loop mode. As can be seen, for the case with $\alpha = 100$, $\beta = 1.5$, the effect increases somewhat, but close to 80% of the power in $u_\delta(t)$ is still linearly correlated with the disturbance. These results are not surprising since, as mentioned previously, a relatively large feedback gain ($K_{\dot{m}}$) in a feedback system such as the inner loop of the dual-loop model will always tend to linearize dynamics in the forward loop.

Figures 11-13 show the amplitude distributions of the control force time histories which yielded Figs. 7 and 9, all obtained from the digital simulation of the dual-loop model over a 120 s run. Note the nearly Gaussian distribution of Fig. 11 compared with the distinctly bimodal distributions of Figs. 12 and 13.

It is also pertinent to investigate the effects of α and β variation upon the form of the dual-loop model describing function Y_p. Serious questions regarding the validity of the modified model would arise if it were shown to yield

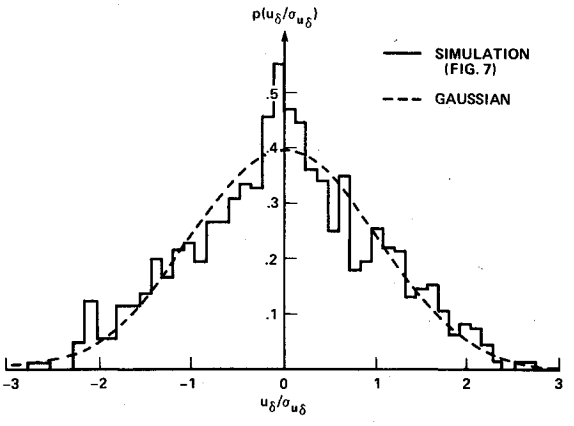

Fig. 11 Amplitude distribution of dual-loop model control force, $Y_\delta Y_c = K/s^2$.

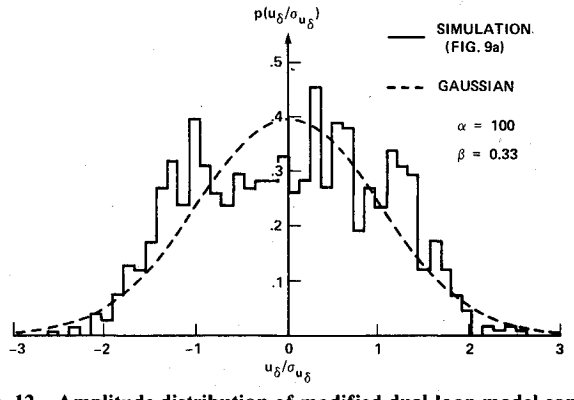

Fig. 12 Amplitude distribution of modified dual-loop model control force, $Y_\delta Y_c = K/s^2$, $\beta = 0.33$.

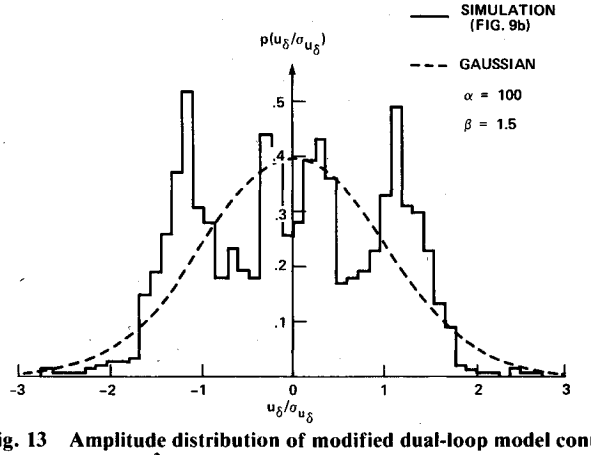

Fig. 13 Amplitude distribution of modified dual-loop model control force, $Y_\delta Y_c = K/s^2$, $\beta = 1.5$.

describing functions which differed considerably from that which a crossover model[1] of the human operator would indicate for similar controlled element dynamics. Figure 14 shows three describing functions obtained from the dual-loop model simulation. These describing functions were computed using a Fourier Transform technique and consist of the amplitude and phase of the nominal Y_p which yielded the time histories of Fig. 7 and that of the two modified Y_p's which yielded the time histories of Fig. 9. As can be seen, the effects of α and β are primarily restricted to high frequencies. For $\alpha = 100$, $\beta = 0.33$, the maximum amplitude in Y_p occurs at approximately 6 rad/s with increased mid- to high-frequency phase lags as compared to the nominal configuration. For $\alpha = 100$, $\beta = 1.5$, a lightly damped neuromuscular mode beyond 10 rad/s is evident, with only a slight change in the

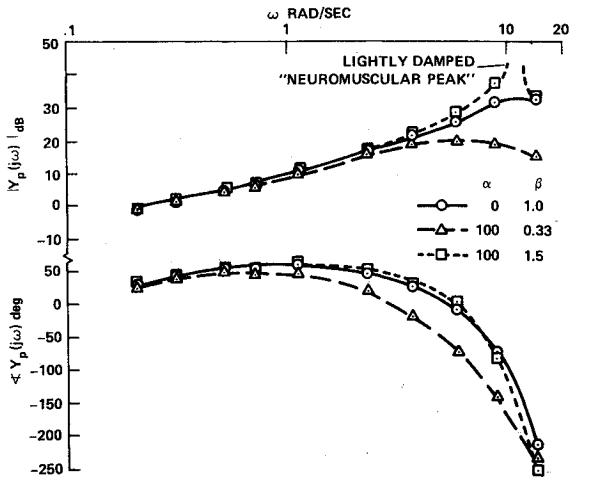

Fig. 14 Computed dual-loop model describing functions, $Y_\delta Y_c = K/s^2$.

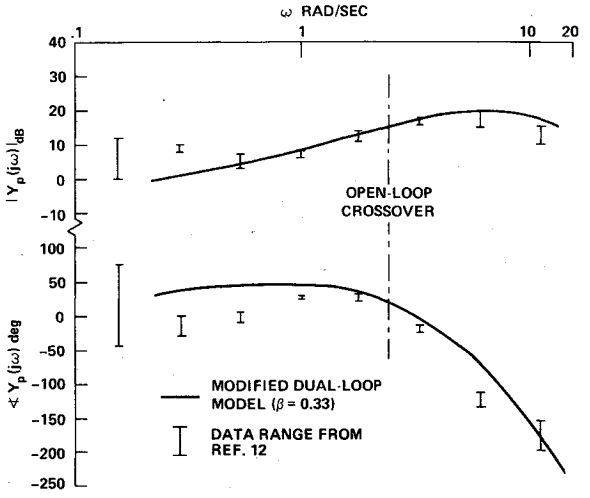

Fig. 15 Measured and dual-loop model describing functions, $\hat{Y}_\delta Y_c = K/s^2$.

phase characteristics as compared to the nominal configuration with $\alpha = 0$, $\beta = 1.0$. Neither of the describing functions for the modified model exhibit characteristics which could be described as anomalous; however, the shape of $Y_p(j\omega)$ for $\beta = 0.33$ is worthy of further discussion.

In Ref. 12, Stapleford et al conducted a pilot-in-the-loop simulation of a jet transport aircraft in a landing approach configuration. A part of the simulation effort, devoted to pitch attitude tracking only, is of interest here since the task variables closely approximate those used to develop pulsive control behavior in the dual-loop model. First, the pitch-attitude to elevator-control vehicle dynamics were essentially $1/s^2$ for $\omega > 1.0$ rad/s (a frequency range which included open-loop crossover). Second, consistent and distinctive pulsive control behavior was adapted by one of the pilots, as evidenced by control output time histories and amplitude distributions. The waveform of the time histories was quite similar to those of Figs. 8a and 9a and possessed an average pulse duration of approximately 1.1 s. Finally, the bandwidth of the pitch command input used in the simulation was comparable to that of the effective command input in Fig. 4c ($-d_3/s$). Thus a comparison of the measured describing function data in Ref. 12 for the pilot who exhibited strong pulsive control behavior and the describing function in Fig. 14 for the digitally simulated dual-loop model with $\beta = 0.33$ is certainly warranted. The comparison is undertaken in Fig. 15.

In Fig. 15, the vertical bars denote the data range for the six runs used in Ref. 12 to obtain the amplitude and phase

measurements of $Y_p(j\omega)$. The solid line is a reproduction of the $\beta = 0.33$ describing function from Fig. 14. The comparison is remarkably good considering that no attempt was made to match the data. Most noteworthy, however, is the fact that the modified dual-loop model exhibits the same amplitude peak in the vicinity of 5-6 rad/s as does the data of Ref. 12. The existence of this peak was somewhat surprising to Stapleford et al., since it occurs at a frequency considerably lower than that normally associated with the neuromuscular system. The authors attributed it to the inertia of the center stick used in the simulation. From what has been discussed here, however, a more detailed model-based explanation could be offered: the relatively low-frequency amplitude peak of Fig. 15 is a natural consequence of a dual-loop human signal processing and control structure. The characteristics of the control stick may indeed be ultimately responsible for the amplitude characteristics of $Y_p(j\omega)$ in Fig. 15, in that the pulsing behavior induced by the K/s^2-like vehicle dynamics might be more easily accomplished at relatively low frequencies (e.g., Fig. 9a) rather than at relatively high frequencies (e.g., Fig. 9b) with a high-inertia stick.

It is finally worth noting that the relative correlated output (ρ_A^2) for the pilot whose data appears in Fig. 15 was reported as 0.36 in Ref. 12. Since Table 3 indicates $\rho_a^2 = 0.95$ for the digitally simulated dual-loop model with $\beta = 0.33$, the nonlinearity Y_{p_u} cannot be considered a significant source of human operator remnant.

Conclusions

1) The interpretation of the inner-loop activity in the dual-loop model of the human operator in terms of the time domain operations of differentiation, multiplication by a constant, or integration leads to a rationale for human operator pulsive control behavior similar to that proposed by Young and Meiry.[3] This rationale is based upon the assumption that the human attempts to reduce the computational burden associated with time integration of sensory inputs. It states that the pulsive control behavior which the human operator often exhibits in controlling K/s^2-like dynamics can be explained as an attempt by the operator to generate control forces which are more easily time integrable than those which would exist in the absence of pulsing.

2) With the addition of a two-parameter nonlinear element, the dual-loop model of the human operator is capable of producing pulsive control force time histories which compare qualitatively with those from a pair of experiments with similar controlled element dynamics. The element does not imply unrealistic or complex information processing and control activity on the part of the human and probably cannot be considered a significant source of human operator remnant.

3) The dual-loop model structure applied to pulsive control behavior appears capable of explaining the existence of the relatively low-frequency "neuromuscular system" amplitude peaks which have appeared in measured describing function data when pulsing is present.

References

[1] McRuer, D.T. et al., "New Approaches to Human Pilot/Vehicle Dynamic Analysis," Air Force Flight Dynamics Laboratory, AFFDL-TR-67-150, Feb. 1968.

[2] Diamantides, N.D., "A Pilot Analog for Airplane Pitch Control," *Journal of the Aeronautical Sciences,* Vol. 25, June 1958, pp. 361-370.

[3] Young, L.R. and Meiry, J.L., "Bang-Bang Aspects of Manual Control in Higher-Order Systems," *IEEE Transactions on Automatic Control,* Vol. AC-10, July 1965, pp. 336-341.

[4] Pitkin, E.T., "A Non-Linear Feedback Model for Tracking Studies," *Proceedings of the Eighth Annual Conference on Manual Control,* May 1972, pp. 11-22.

[5] Smith, R.H., "A Unified Theory for Pilot Opinion Rating," *Proceedings of the Twelfth Annual Conference on Manual Control,* May 1976, pp. 542-558.

[6] Smith, R.H., "A Theory for Handling Qualities With Applications to MIL-F-8785B," Air Force Flight Dynamics Laboratory, AFFDL-TR-75-119, Oct. 1976.

[7] Hess, R.A., " Dual-Loop Model of the Human Controller," *Journal of Guidance and Control,* Vol. 1, July-Aug. 1978, pp. 254-260.

[8] Granit, R., *The Basis of Motor Control,* Academic Press, London and New York, 1970, Chaps. III and V.

[9] Eyzaguirre, C. and Fidone, S.J., *Physiology of the Nervous System,* 2nd Ed., Year Book Medical, Chicago, 1975, Chap. 13.

[10] Kleinman, D.L., Baron, S., and Levison, W.H., "An Optimal Control Model of Human Response, Part I," *Automatica,* Vol. 6, 1970, pp. 357-369.

[11] McRuer, D.T. and Graham, D., *Analysis of Nonlinear Control Systems,* Wiley, New York, 1961, pp. 104-134.

[12] Stapleford, R.L., Craig, S.J., and Tennant, J.A., "Measurement of Pilot Describing Functions in Single-Controller Multiloop Tasks," NASA CR-1238, Jan. 1969.